Physica B 667 (2023) 415199

Contents lists available at ScienceDirect

Physica B: Condensed Matter

journal homepage: www.elsevier.com/locate/physb

Structural, optical and magnetic studies of sol-gel synthesized Mg-doped pure anatase TiO_2 nanoparticles for spintronic and optoelectronics applications

O. Adedokun [a,b,*], P. Sivaprakash [c], A.S. Ajani [d], I.T. Bello [e], S. Arumugam [c,**]

[a] Department of Pure and Applied Physics, Ladoke Akintola University of Technology, P.M.B 4000, Ogbomoso, Nigeria
[b] Nanotechnology Research Group (NANO+), Ladoke Akintola University of Technology, Ogbomoso, Nigeria
[c] Centre for High Pressure Research, School of Physics, Bharathidasan University, Tiruchirappalli, 620 024, Tamil Nadu, India
[d] Department of Physics and Material Science, Faculty of Pure and Applied Sciences, Kwara State University, Malete, P.M.B 1530, Ilorin, Kwara State, Nigeria
[e] Department of Physics, College of Science, Engineering and Technology, University of South Africa, Johannesburg, 1710, South Africa

ARTICLE INFO

Keywords:
Sol-gel synthesis
Mg doped TiO_2
RTFM
Structural properties
Optical properties
Magnetic properties

ABSTRACT

Here in we reported the synthesis of $Mg_xT_{1-x}O_2$ (for x = 0.00, 0.01, 0.02, 0.03, 0.04) nanoparticles via simple sol-gel technique. Mg-doped TiO_2 is a hopeful material for the study of the origin of room-temperature ferromagnetism (RTFM) in dilute magnetic semiconductors (DMS) systems, but very scanty work on this material has been reported. The as-synthesized samples were subjected to X-ray diffraction (XRD) which shows that the samples aligned with tetragonal anatase phase of TiO_2. UV\Vis\NIR diffuse reflectance spectroscopy analysis showed a slight increase in TiO_2 energy band gap with Mg doping from 3.25eV to 3.33 eV as a result of blue shift in absorbance edge of the sample. The obtained recombination of photo-generated electrons and holes is excellently curbed by Mg doping which was examined by the photoluminescence study and the blue shift in the most intense Eg (3) Raman mode confirms integrated Mg in TiO_2 lattice. As revealed by Field Emission Scanning Electron Microscopy (FESEM), the morphology of the samples showed irregularly distributed nanoparticles and to examine elemental composition of the samples, Energy Dispersive X-ray (EDX) were carried out which stipulates all elements like Ti and Mg are in the sample. Soft ferromagnetism at low magnetic field with hysteresis loop was noticed in all the samples, with values of coercivity in the range 206–309Oe. Maximum value of saturation magnetization was evident by the 2% doped sample. These materials can find applications in electronics, spintronics and magneto-optics devices.

1. Introduction

Over the years, the world economy is growing and the progress in miniaturization of electronics devices has contributed immensely to the continuous technological advancement, improving the performance and speed of the information exchange. Several growing interests have been developed in nanostructured semiconductors owing to their important roles in optical, magnetic, electrical and catalytic applications. Semiconductor nanoparticle is a unique material with many remarkable properties. There are several unprecedented new devices fabricated by these nanoparticles [1–7]. Titanium (IV) oxide (TiO_2) is a wide band gap nanostructured type of functional material utilized in various applications such as in photocatalysis [8], dye-sensitized solar cells [3,7], lithium-ion batteries [6] and dilute magnetic semiconductors (DMS) [4,5]. DMSs have allured much attention due to their hopeful potential applications in future spintronics and magneto-optic devices, where they combine semiconducting and ferromagnetic behavior at room temperature within the same material [9]. Despite the discovery of stable ferromagnetism above room temperature in Co-doped TiO_2 thin films [10], several transition metals (TM) (for instance Fe, Ag, Ni, Co, Cr, Mn), oxides of doped metal semiconductor (for instance TiO_2, ZnO and SnO_2) have been widely studied [4,5,7,9–16]. Among these metal oxides, TiO_2 nanoparticles have been broadly examined owing to their non-toxicity in nature, high stability, cheap, photo-catalytic, electronic and magnetic properties [13]. The modification of synthesis conditions through appropriate doping of nanostructured TiO_2 provide a pathway

* Corresponding author.Department of Pure and Applied Physics, Ladoke Akintola University of Technology, P.M.B 4000, Ogbomoso, Nigeria.
** Corresponding author. Centre for High Pressure Research, School of Physics, Bharathidasan University, Tiruchirappalli, 620024, Tamil Nadu, India.
E-mail addresses: oadedokun@lautech.edu.ng (O. Adedokun), sarumugam1963@yahoo.com (S. Arumugam).

https://doi.org/10.1016/j.physb.2023.415199
Received 12 April 2023; Received in revised form 18 July 2023; Accepted 6 August 2023
Available online 10 August 2023
0921-4526/© 2023 Elsevier B.V. All rights reserved.

towards tailoring its energy bandgap and enhancement of saturation magnetization, thus creating avenue for magneto-optoelectronic applications. These have long become the key area of research which has attracted more attention [11]. TiO_2 crystallizes into anatase, rutile and brookite crystallographic phases. From these crystallographic phases, anatase is a stable phase till 600 °C and it converts into rutile phase at higher temperature while the brookite phase is very unstable. Several techniques have been deployed for the preparation of undoped and doped TiO_2 nanoparticles which involve the sol–gel procedure [5,11,17], sputtering [18], electrochemical anodization [19], chemical vapor deposition [20], pulsed laser ablation [21], hydrothermal method [22], etc. In the midst of the current techniques, sol–gel technique is a facile route of synthesizing diverse oxide of metal materials. The sol–gel proffers an edge for an efficient process for accurately controlling the stoichiometry, simple control of concentration of the metal dopant, a low-temperature preparation method that give high purity and crystallinity samples [23]. The optical and structural properties of TiO_2 nanoparticles are greatly modified by tuning their band gaps by doping with transition metals (Co, Fe, Ag, Ni, Mn) [7,11,14,23], nonmetals (F, B, C, N) [9,24], rare earth elements (La, Gd) [25,26], alkaline earth metals (Sr, Mg) [27,28] and post transition metals (B, Al, Bi) [29–31] and so on, that promote the photocatalytic activity in visible region which stipulates opto-electronic device applications potential. The preparation methods, presence of defects, shape and size of the TiO_2 nanoparticles and their interaction contribute a strong part in the magnetic characteristics of doped TiO_2 [26]. Ahmed et al. [14] reported in their work the role of defects for the stability of ferromagnetism in Mn-doped TiO_2. TiO_2 nanoparticles do show a wide range of magnetic characteristics, which may range from ferromagnetism then to paramagnetism, and to superparamagnetism or diamagnetism based on dopant ions type, owing to different kind of magnetic ordering in their systems during addition of dopants. Matsumoto et al. [10] reported the first FM above room temperature in Co-doped TiO_2. Since then, several considerable studies have been reported on the preparation and magnetic studies of TMs doped TiO_2-based DMSs. TiO_2 doped with various magnetic ions for achieving room-temperature ferromagnetism (RTFM) is one of the attractive areas of research due to their potential applications. However, the RTFM source is often contentious and even conflicting, especially pertaining the role that could be played by magnetic impurities and the strong correlation observed between RTFM and the presence of defects (either during synthesis or doping with nonmagnetic element). The RTFM properties of transition metal-doped TiO_2 may be observed due to precipitation of magnetic clusters or second phase [23,24]. These forms of extrinsic magnetic behavior are undesirable for practical application. This challenge of magnetic precipitation is surmountable and could be resolved using an element that is intrinsically nonmagnetic and can be integrated easily into metal oxide to form DMSs as dopant. Few reports on nonmetal, N, C-doped TiO_2 standing on first principle calculations gave predictions of the possibility of holes-induced RTFM [23,24]. But in reality, it is difficult to prepare doped anatase TiO_2 with anion site doping owing to its synthesis process dependency. In addition, the substitution of low valence metals into a tetravalent titanium site in TiO_2 also may create holes in the O 2p band [32]. Therefore, Mg-doped TiO_2 is a hopeful material for the study of the origin of RTFM in DMS systems, but very scanty work on this material has been reported except the theoretical work of Liu et al. [33], and experimental work of Ali et al. [34] and Chouhan and Srivastava [35]. Optical and RTFM of Mg-doped TiO_2 by density functional theory (DFT) was reported by Ref. [33]. He gave a prediction that the spin-polarization in Mg-doped anatase TiO_2 is not the same with that in other oxides and Mg tends to favor the FM coupling which is stable at room temperature. Experimentally, RTFM of Mg-doped TiO_2 were reported by Refs. [34,35]. Ali et al. reported a very weak saturation magnetization for room temperature ferromagnetism in both undoped and Mg-doped anatase TiO_2 material using cost effective sol-gel method [34]. The combined phases of rutile and anatase Mg-doped TiO_2 compounds were then prepared by that of standard solid state reaction pathway by Chouhan and Srivastava. From all the Mg-doped TiO_2 reported, RTFM is being reported with Curie -temperature over 400 K and synthesized materials display zero dielectric loss and a significant dielectric constant [35]. In order to achieve more insights into the origin of the FM observed in Mg-doped TiO_2 systems, we investigate the effects of Mg concentration on magnetic properties of $Mg_xT_{1-x}O_2$ nanoparticles powder samples. Therefore, we attempt to synthesize and study the structure, morphology, magnetic behaviour and optical properties of undoped and Mg-doped titanium dioxide nanoparticles prepared through a simplified sol-gel method, that the final product could find potential applications in spintronics and magneto-optic devices.

2. Experimental details

2.1. Materials

Titanium (IV) isopropoxide (TTIP) (SRL India; extrapure 27.8–28.6% TiO_2) and magnesium sulphate heptahydrate (SRL India; extrapure AR, 99%) were employed as precursors basements for titanium and magnesium respectively. As solvent, Isopropanol (SRL India; extrapure AR, 99.5%) and ethylene-glycol (SRL India; extrapure AR, 99%) were respectively employed while acetic acid glacial (SRL India; extrapure AR, 99.9%) was employed as a catalyst and deionized water (DI) (Royal India; >99% pure) was employed for hydrolysis to initiate the formation of the gel. All the reagents employed in this work were of an analytical grade and used without any further purifications.

2.2. Synthesis of undoped and doped TiO_2 nanomaterials

All the powder samples of undoped and Mg doped TiO_2 nanoparticles were prepared through a simple sol-gel method. In a typical preparation of pure and doped TiO_2, solution A and B were firstly prepared and stirred separately for 30 min. Solution A was made from 5 mL TTIP, 10 mL of glacial acetic acid and 10 mL isopropanol. Solution B comprised of 60 mL DI, 10 mL Isopropanol and 5 mL ethylene glycol. Solution B was added to solution A dropwisely with vigorous stirring and stirred more for 1 h at 90 ± 2 °C. The time of gelation as well as the grain size is being controlled by the amount of DI water used [5]. In order to reduce the gelation time, the molar ratio between TTIP: acetic acid: DI water was kept at 1:10:200 respectively, for all the prepared samples. The resulting sol-gel solution was left for few hours and later dried at 200 ± 2 °C for 3 h. The Mg doped TiO_2 was prepared by the similar procedure with Mg/Ti molar ratio of 0, 1, 2, 3, and 4% being added into solution B to obtain the required doping concentration for samples labeled as MT-0, MT-1, MT-2, MT-3 and MT-4, respectively. In order to improve the crystallinity of the final powder products, the resulting powder samples of intrinsic and Mg doped TiO_2 were annealed in air at 500 °C for 4 h.

2.3. Characterization

The crystal structures and the phase information of all powder samples were evaluated with powder X-ray powder diffraction using Rigaku X-ray diffractometer (Smartlab) with X-ray generator operating at 40 kV and 30 mA. The XRD measurements were obtained by step scanning method over 2θ range from 20° to 80° with a step range of 0.01° and a scanning speed of 2.016°/min. The Renishaw Raman spectrometer with the 532 nm red laser was used for the structural analysis. The Raman signal was collated in the spectral interval of 100 per cm until 1500 per cm. The Raman shift and intensities of the dispersed light were compared with reference data. Fourier transform infrared (FTIR) spectroscopy was conducted using Model Shimadzu IR Affinity FTIR 8400S spectrometer within wavenumber between 4000 and 400 cm^{-1} in order to evaluate surface chemistry and functional group of undoped and magnesium doped TiO_2 samples. The optical reflectance and transmittance data were recorded employing a U–V visible

spectrophotometer integrated with diffuse reflectance attachment as integrating sphere (Ocean-Optics USB 4000 spectrometer in the wavelength range of 200–800 nm) for the synthesized nanoparticle. The room-temperature photoluminescence spectra for the undoped and magnesium doped TiO_2 samples are recorded on Elco spectrometer SL174. The particles' shape, morphological behavior, and distribution were examined through FESEM-field emission scanning electron microscopy (FESEM, Zeiss Ultra 55) with an Energy-Dispersive X-ray spectrometer. The magnetic measurements were taken by Physical Property Measurements System coupled with Vibrating Sample Magnetometer (PPMS –VSM) module (Quantum Design, USA) was employed for magnetic measurements with a determined magnetic field of 8 kOe.

3. Results and discussion

3.1. Structural analysis

3.1.1. X-ray diffraction analysis

In order to study the crystal structure of undoped TiO_2 and Mg doped-TiO_2 with different concentration, XRD analysis was carried-out on all the prepared samples. The XRD pattern of the prepared $Mg_xT_{1-x}O_2$ (for x = 0.00, 0.01, 0.02, 0.03, 0.04) nanoparticles are displayed in Fig. 1(a). The XRD analysis showed that diffraction peaks for all the samples were arranged to tetragonal anatase phase of Titanium dioxide with space group $I4_1/amd$ (JCPDS PDF # 73–1764). There is no presence of any impurity phases corresponding to MgO within the XRD detection limit. The shift in diffraction peak and a broadening of the most intense peak (101) towards lower diffraction angles (2θ) with increasing Mg doping concentration was observed in XRD patterns as depicted in Fig. 1(b). Effect like this could be ascribed to the substitution of ion by slightly higher radius in the lattice site bringing about the effect of stress or strain in the prepared samples because Mg^{2+} ion has a comparable ionic radius of 0.72 Å (Mg^{2+}) to that of 0.61 Å (Ti^{4+}) within the $Mg_xT_{1-x}O_2$ system, without much distortion to the TiO_2 structure as reported by Olowoyo et al. [29]. The synthesized crystallite size of the samples was calculated from Scherer's equation (Eqn. (1)) by considering the instrumental widening from the XRD patterns of the Bragg peak as a combination of both instrumental and sample dependent effect [36–39]. The corrected broadening correlated with the most intense diffraction peaks of the prepared samples were evaluated using the expression in Eqn. (2).

$$D = \frac{K\lambda}{\beta_{hkl}\cos\theta} \tag{1}$$

$$\beta_{hkl} = \left[(\beta_{hkl})^2_{measured} - (\beta_{hkl})^2_{Instrumental}\right]^{½} \tag{2}$$

where D is the crystallite size, K is given as constant equal to 0.90, λ is the wavelength of the incident X-rays (λ = 1.540 Å), β_{hkl} is full-width-at-half-maximum (FWHM, in radian) of the most intense peak at diffracting angle θ of the sample, *and* θ the Bragg's angle position in degree. The Willliamson and Smallman formula [36,37,39] was used to calculate the dislocation density and lattice strain. A summary of crystallographic parameters from XRD analysis for the $Mg_xT_{1-x}O_2$ (x = 0.00, 0.01, 0.02, 0.03, 0.04) nanoparticles is tabulated as Table 1. Table 1 reveals that a decrease in crystallite size and increase in dislocation density and lattice strain in the synthesized samples were noticed with an increase of Mg doping impurity. The decrease in average crystallite size observed as the concentration of Magnesium doping increases as given in Fig. 1(c) can be attributed to formation of Mg–*O*–Ti bonds which impedes nucleation and nanoparticles growth [29,34,35].

This indicates that Ti^{4+} ion have been replaced by Mg^{+2} as the ions inside the host lattice of TiO_2 which then leads to decrease of the average

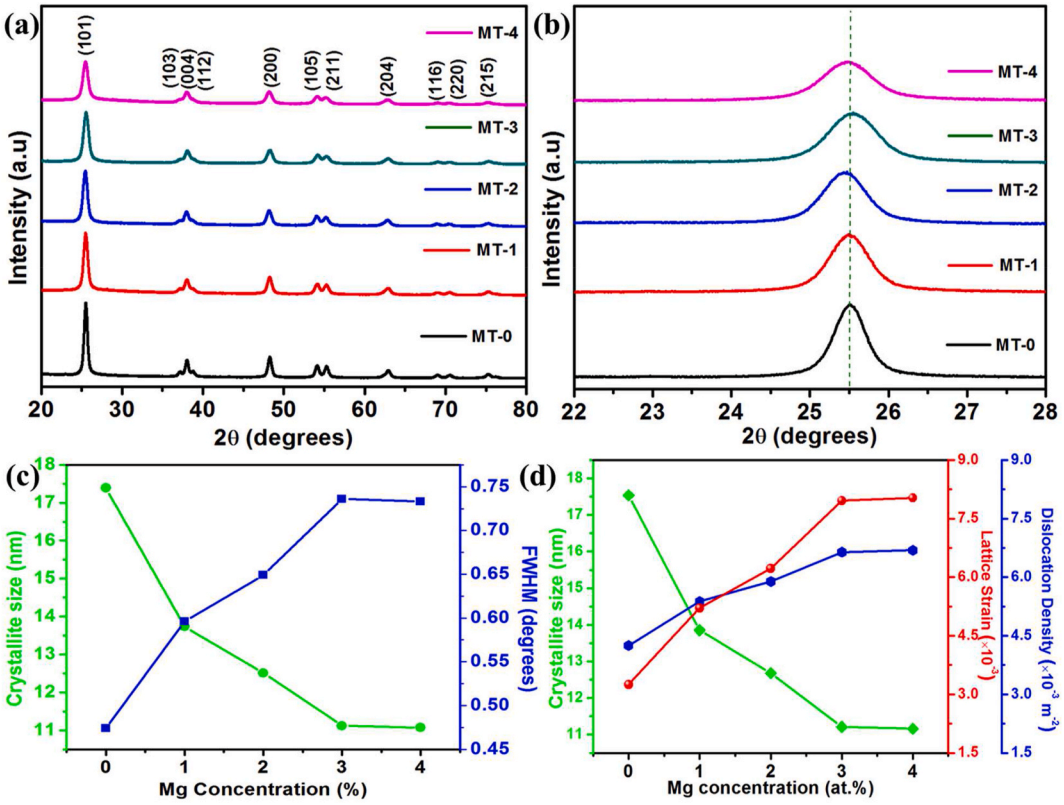


Fig. 1. a). X ray -Powder Diffraction -XRD spectra of Mg-doped TiO_2 nanoparticles. b) Peak shift corresponding to (101) peak in MT-0, MT-1, MT-2, MT-3 and MT-4. c). Evaluated Variation of crystallite size with Scherrer's formula and full-width-at-half-maximum - FWHM corresponding to each of the samples. d). The variation of crystallite-size and lattice strain generated from a size-strain plot against the concentration of Mg.

Table 1
Evaluated lattice constants *(a, c),* microstructure parameters, crystallite size *(D),* volume of unit cell *(V)*, and lattice strain estimated from XRD analysis for Mg-doped TiO_2 nanoparticles.

Sample	Molar Conc. of Mg^{2+} (%)	D Spacing (Å)			Lattice Parameters			Cell Volume (V) ($Å^3$)	FWHM (degree)	Crystallite size (nm)		Lattice Strain ($\varepsilon \times 10^{-3}$)
		(101)	(200)	(004)	a (Å)	c (Å)	Ratio c/a			Scherer's method	W–H plot	
MT-0	**0.00**	**3.4907**	**1.8857**	**2.3663**	**3.771**	**9.465**	**2.510**	**134.596**	**0.464**	**17.54**	**14.43**	**1.36**
MT-1	**0.01**	**3.4909**	**1.8869**	**2.3672**	**3.774**	**9.469**	**2.509**	**134.868**	**0.588**	**13.85**	**13.19**	**1.09**
MT-2	**0.02**	**3.4998**	**1.8893**	**2.3669**	**3.779**	**9.468**	**2.505**	**135.211**	**0.642**	**12.69**	**11.16**	**1.43**
MT-3	**0.03**	**3.4846**	**1.8852**	**2.3581**	**3.770**	**9.432**	**2.502**	**134.056**	**0.729**	**11.16**	**9.39**	**2.06**
MT-4	**0.04**	**3.4975**	**1.8867**	**2.3721**	**3.773**	**9.488**	**2.515**	**135.067**	**0.727**	**11.21**	**9.52**	**0.94**

crystallite size. The plot of crystallite size against both of lattice strain and dislocation density is shown in Fig. 1(d). Decrease in crystallite size and increase in lattice strain with dislocation density in the samples have been observed with an increase of Mg doping. This increase of both lattice strain and dislocation density could be the reason for the broadening of XRD peak, contrast in FWHM and decrease in crystallite size with increasing in Mg concentration.

Fig. 2 shows Rietveld refinement of the XRD patterns using GSAS 2 software. Rietveld refinement confirms that Mg-doped TiO_2 crystallizes in the anatase tetragonal structure. There is observation of slight variation in lattice parameters, as well as unit cell volumes, as observed with increasing Mg concentration which can be attributed to the larger ionic radius of Mg^{2+}ions (0.72 Å) compared to that of Ti^{4+}ions (0.61 Å) [11]. This difference in the ionic radii of $Mg^{2+}$and Ti^{4+} might have cause the small enhancement of the TiO_2 unit cell volume [11] The XRD detailed analysis gives the information that Mg ions have substituted the Ti ions and the plot of size-strain presents that the change in FWHM is possibly due to the lattice strain associated with the doped TiO_2 samples.

3.1.2. The Raman spectroscopy

It is well recognized that Raman spectroscopy technique is one of the crucial and non-destructive tools to identify the crystallinity and defects structure of nanomaterials [40]. The effect phonon confinement and non-stoichiometry in nanomaterials has a significant effect on the change of Raman spectra. Oxygen deficiency within the material, however, strongly affects the Raman spectrum by producing shifting and broadening of some spectral peaks [41]. The Raman spectra of intrinsic and Mg doped TiO_2 are shown in Fig. 3(a) and matched with tetragonal phase of anatase TiO_2. The bands of TiO_2 appeared at lower frequency Raman region. The TiO_2 is exhibiting Raman bands at 144, 396, 515, and 639 cm^{-1}, corresponding to Eg (1), B_1g, A_1g and Eg (3) modes [40], as shown in Fig. 3(a). The most intense characteristic peak of the MT-0 has a blue shift towards a higher wavelength in MT-1, MT-2, MT-3 and MT-4 respectively, which may be attributed to phonon confinement. Kumar et al. (2017) reported a similar shift [42]. There is decrease in the intensity of the Raman peaks for MT-1, MT-2, MT-3 and MT-4 when compared with MT-0. This is due to the disorder of induced lattice of TiO_2 by Mg. Also, the Eg (3) Raman mode shows a blue shift for MT-1, MT-2 and MT-3 (640, 641, 641 cm^{-1}) while there is a redshift for MT-4

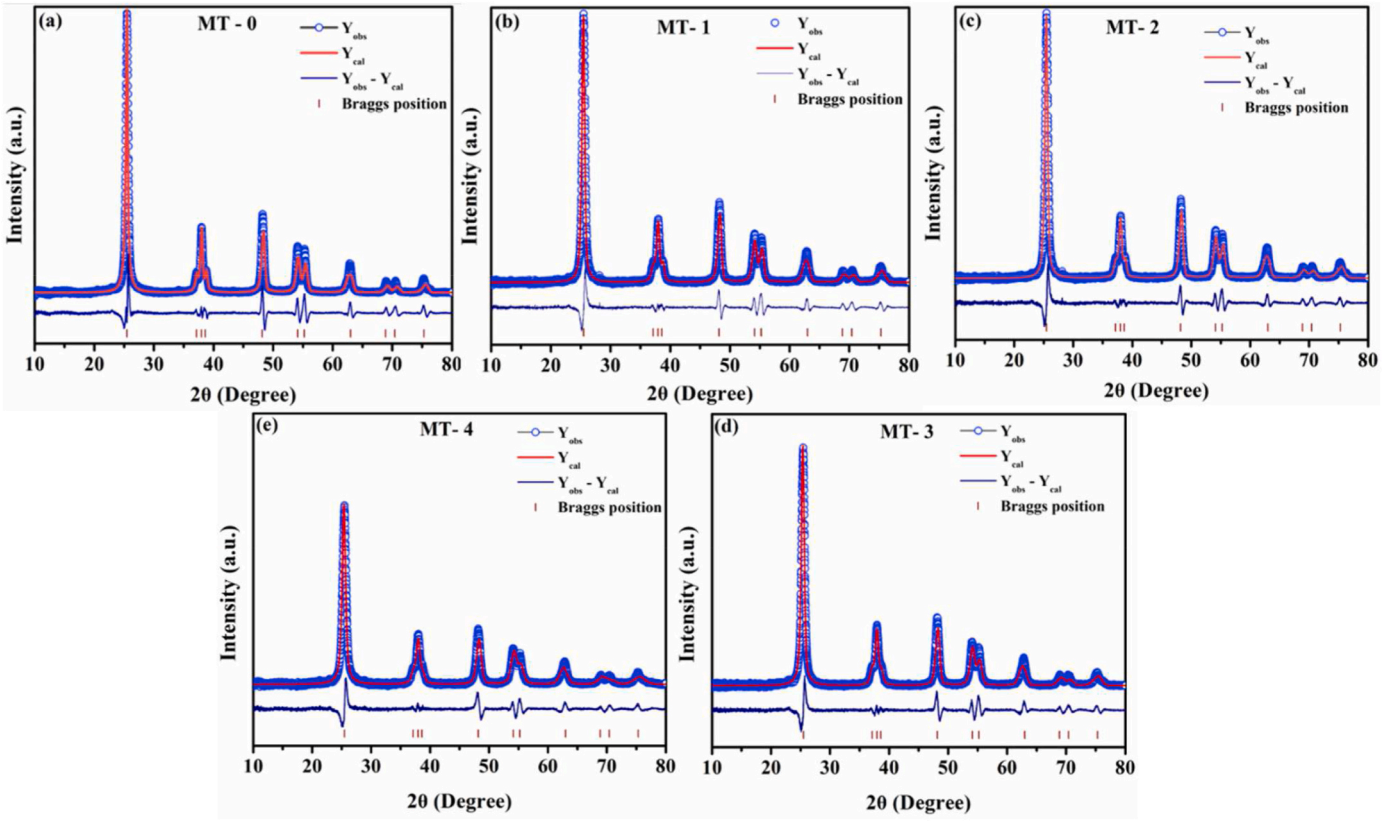


Fig. 2. Rietveld Refinement plots of MT-0, MT-1, MT-2, MT-3 and MT-4.

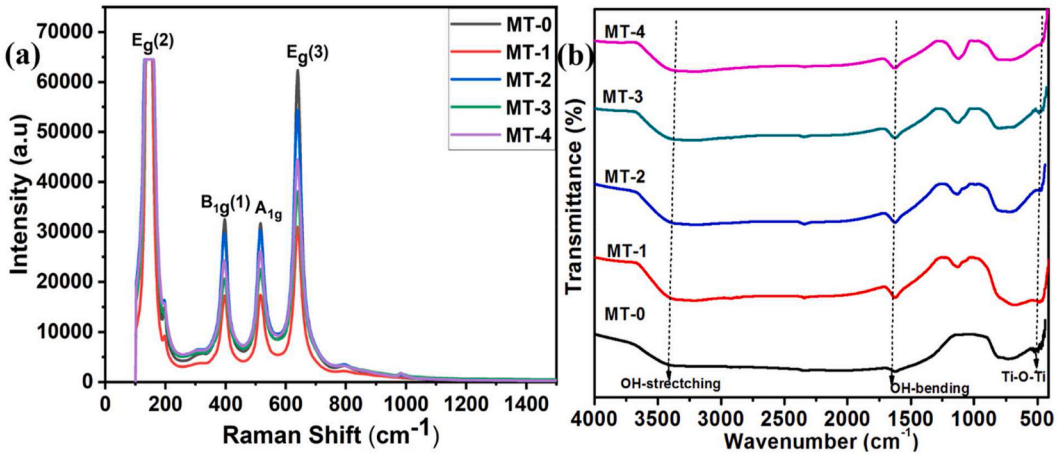


Fig. 3. (a) Plot of Raman spectra (b) FTIR spectra of MT-0, MT-1, MT-2, MT-3 and MT-4.

(638 cm^{-1}). This result indicates compressive strain in MT-1, MT-2, MT-3 and tensile strain for MT-4 which is associated to Mg doping in lattice of TiO_2. Hence, this Raman spectra analysis shows that Mg dopant a significant effect on TiO_2 lattice vibration.

3.1.3. FTIR studies

FTIR spectra of $T_{1-x}Mg_xO_2$ (x = 0.00, 0.01, 0.02, 0.03, 0.04) NPs are measured and plotted as displayed in Fig. 3(b). FTIR spectra of undoped and Mg doped TiO_2 displayed peaks corresponding to stretching vibrations of O–H from hydroxyl and bending vibrations of adsorbed of molecules water around 2964–3402 cm^{-1} and 1628 cm^{-1}, respectively. The strong absorption at lower energy region below 500 cm^{-1} of broad characteristics band is due to the Ti–O–Ti vibration lattice formation [43,44]. This peak has been red shifted to 482.46 cm^{-1} in Mg-doped TiO_2 which may correspond to the band stretching of magnesium in lattice structure of Ti–*O*–Mg–Ti vibration. The result of FTIR clearly stipulates the Mg as doping impurities present in Mg doped TiO_2 structure. Hence the FT-IR analysis agrees with the XRD and Raman studies which established the substitution of Mg^{2+} into TiO_2 lattice.

3.2. Optical properties

3.2.1. UV/Vis/NIR diffuse reflectance spectroscopy

To understand the structure band and energy band gap of the syn-

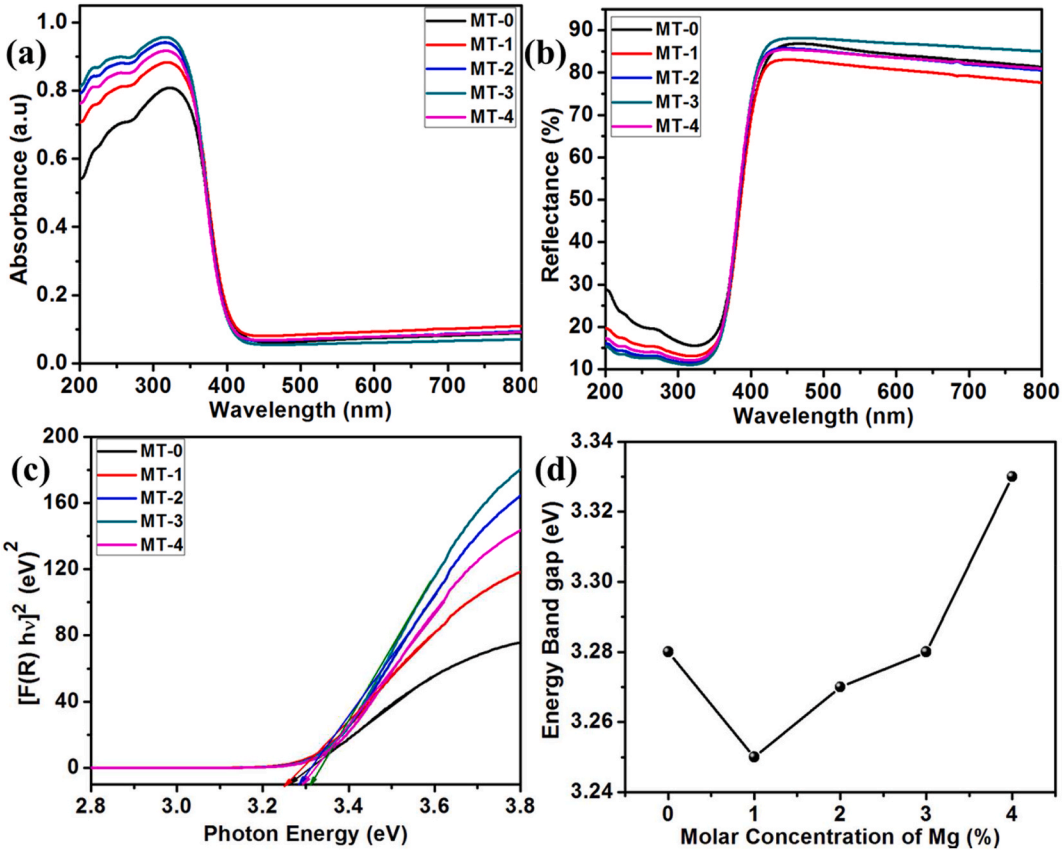


Fig. 4. (a) UV–Vis absorption spectra (b) diffuse reflectance spectra measured for $T_{1-x}Mg_xO_2$ (x = 0.00, 0.01, 0.02, 0.03, 0.04) nanoparticles with (c) corresponding Tauc plots with (d) the changed in energy band-gap with Mg concentration.

thesized powder samples at different molar concentration of Mg doping, the band gap features were obtained by UV–Vis–NIR spectrophotometer in Diffuse Reflectance Scattering (DRS) condition at ambient temperature between 200 and 800 nm. The $Ti_{1-x}Mg_xO_2$ optical absorption-spectra of the samples were converted and recorded from diffused reflectance spectral employing the Kubelka-Munk (K-M) function F(R) in Eqn. (3).

$$F(R) = \frac{K}{S} = \frac{(1-R)^2}{2R} \tag{3}$$

where R denotes the diffuse reflectance of the sample, K is the corresponding K–M absorption and S is the scattering coefficient. UV–Vis absorption spectra measured and recorded for $T_{1-x}Mg_xO_2$ (x = 0.00, 0.01, 0.02, 0.03, 0.04) NPs are shown in Fig. 4(a). It is shown that maximum absorbance value of synthesized samples increases with Mg doping concentration with a fundamental absorption edge centered at 320 nm for undoped TiO_2 and slightly shifted to lower wavelength (between 316 and 318 nm) for Mg doped TiO_2 which is consistent with the reported work on Mg doped TiO_2 [43,44]. This could be attributed to the replacement of Mg ion in Ti sites, and this is slightly modifying the band structure and thus the fundamental absorption edge shifted to higher photon energy for doped TiO_2 NPs. Diffuse reflectance spectra (DRS) of undoped and Mg-doped TiO_2 NPs are shown in Fig. 4(b). The pure anatase TiO_2 gives high reflectance of 85.4% at 480 nm and displayed a decrease but almost consistent value from 86.4 to 84% over wavelength range 400–800 nm. This slightly high reflectance obtained from pure TiO_2 established actual common trend of TiO_2 which is one of the most suitable materials considered in the field of cool pigments [5]. There is slight decrease in reflectance by addition of Mg doping (at 1%) over wavelength range 400–800 nm and which is then slightly increase with higher Mg concentration (at 3%). This slight change could be attributed to different energy levels formation in band gap of the synthesized samples. The value of optical band gap near the absorption edge could be obtained using the relationship between band gap and absorption coefficient as given by Tauc equation [45]:

$$(\alpha h\nu) = A\left(h\nu - E_g\right)^n \tag{4}$$

where α is the absorption coefficient of the sample, $h\nu$ is the photon energy, A is a constant, E_g is the energy band gap and n is constant for a given transition equal to 2 and $\frac{1}{2}$ for allowed indirect and direct band gap material, respectively. Let us assume the material scatters light in a perfectly diffuse manner, K–M function could be expressed similar to Tauc's equation as:

$$F(R)h\nu = A\left(h\nu - E_g\right)^n \tag{5}$$

The band gap was obtained from direct transition by plotting $(F(R)h\nu)^2$ as against $h\nu$ while extrapolating the graph to the point where $F(R) = 0$ is known as energy band gap. The band gap energies of all the synthesized samples are shown in Fig. 4(c). We observed slight increase in energy band gap with Mg doping from 3.25eV to 3.33 eV. This shows that Mg doping ensued with a trifling blue shift of the absorption edge which reckoned for the broadening of the band gap by influencing the conduction bandwidth and the valence band thereby increasing enclosure energy with decrease in particle sizes [29,46]. The energy band gap formation in $T_{1-x}Mg_xO_2$ is originated from the enhanced state ascribed to the higher energy level in the Mg 3s orbital to that of Ti 4s orbital which sweeps the conduction band upwards while Ti 4d and O 2p orbitals in the valence band due to repulsion effect between lower and upper levels are accountable for the variation of optical band gap resulting to higher energy of the doped TiO_2 synthesized samples. The energy band gap of $T_{1-x}Mg_xO_2$ (x = 0.00, 0.01, 0.02, 0.03, 0.04) NPs as a function of Mg doping is plotted are described in Fig. 4(d).

3.2.2. Linear and nonlinear optical studies

The linear and nonlinear optical parameters is very important to ascertain the potential of using the materials in optoelectronic, photovoltaic and devices applications. Linear optical parameters like absorption and extinction coefficient, skin depth, refractive index, optical dielectric constant and dielectric loss tangent were evaluated from this study. Absorption coefficient (α) is defined as the decrease of the electromagnetic light intensity as a result of its absorption and can be calculated considering using the following relation [47,48]:

$$\alpha = \frac{(1-R)^2}{2R} \tag{6}$$

where R represent reflectance. The dependency of Skin depth (δ) to absorption coefficient is given as $\delta = \frac{1}{\alpha}$, which is the depth at which intensity of photon decays to $\frac{1}{e}$ of its initial value on the surface of the material [49].

The values of the extinction coefficient (k) have been calculated using the relation

$$k = \alpha\frac{\lambda}{4\pi} \tag{7}$$

where λ is the wavelength [47].

Fig. 5(a, b, and c) indicate the spectral dependencies of optical parameters (absorption and extinction coefficient, and skin depth). Both absorption and extinction coefficient spectra obviously give similar spectra and their values increase at higher value of photon energy. Hence, the absorption and extinction coefficient exhibit an increasing behavior with increasing photon energy (decreasing in wavelength). However, the skin depth value decreases as the photon energy increases to higher value of 3.3–4.5 eV. The skin depth also exhibits a decreasing behavior with increasing photon energy (decreasing in wavelength).

The refractive index of the samples is crucial for evaluating the optoelectronic behaviour of the material. The refractive index depends on the reflectance and is independent of the absorbance of the material [49]. The refractive index of the sample is evaluated using the.

following relation [47,48]:

$$n = \frac{1+R}{(1-R) + \left(\sqrt{\left({}^{4R}/_{1-R^2-k^2}\right)}\right)} \tag{8}$$

The dispersion of the refractive index for undoped and Mg doped TiO_2 nanomaterial is illustrated as shown in Fig. 5(d). Fig. 5(d) shows the behavior of refractive index with photon energy for the obtained Mg doped TiO_2 nanomaterial. There is obvious increase of the refractive index with increase of photon energy (decrease in wavelength). This is known as normal dispersion. As observed from the spectra, normal dispersion appears below the ~2.0 eV [49]. The calculation of the dispersion parameters takes essential role to have a foresight about usage potential of the material in optoelectronic applications. It is observed from Fig. 5(d) also that as Mg concentration increased the refractive index of the prepared Mg–TiO_2 increased at higher photon energy (lower wavelength). The increasing of the refractive index may be attributed to the decrease in the carrier density and interfacial states in Mg–TiO_2 samples [48,49].

The dielectric constant is related to the refractive index via the following equation [47–49]:

$$\varepsilon_1 + i\varepsilon_2 = (n^*)^2 = (n+ik)^2 \tag{9}$$

$$= n^2 - k^2 + i2nk \tag{10}$$

The real and imaginary parts of the dielectric constants' values were evaluated and plotted against the photon energy, as shown in Fig. 6(a and b). Furthermore, based on the very low obtained values of the extinction coefficient ($k \ll R$), k^2 in eqn. (10) is nearly has no effect on

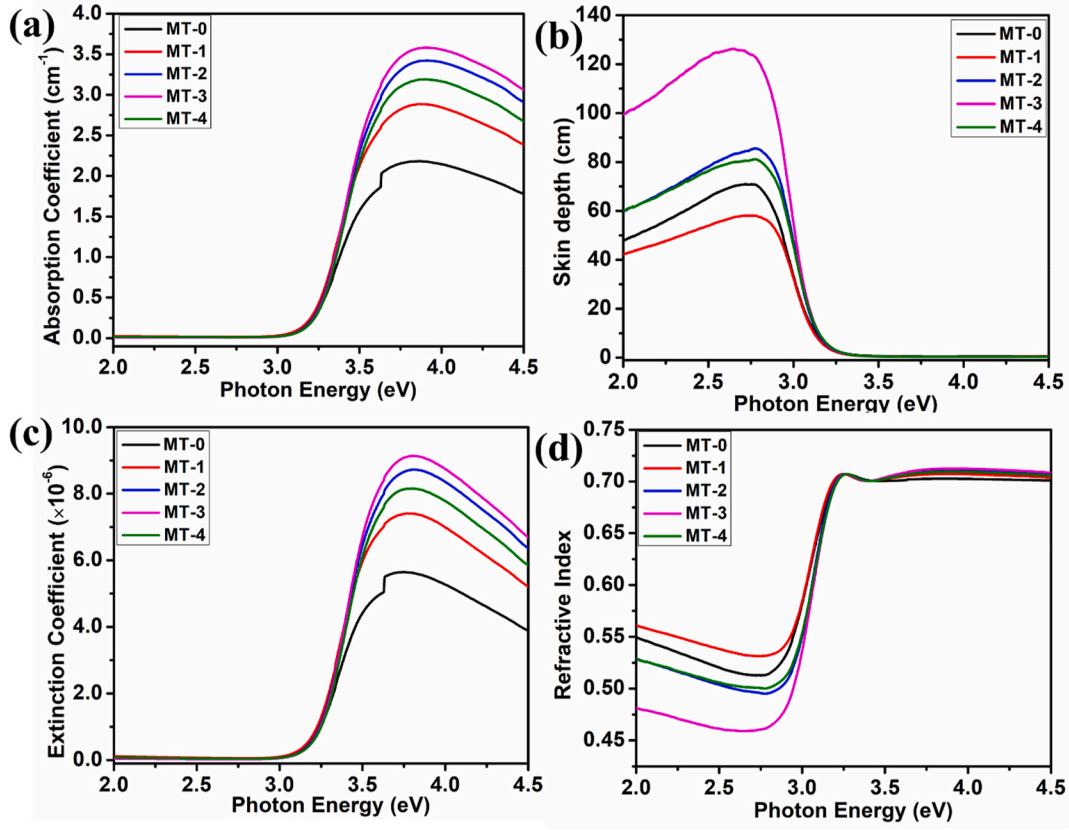


Fig. 5. (a) Absorption coefficient, α (b) Skin depth, δ (c) Extinction coefficient, k and (d) The dispersion of the refractive index (n), spectra for $T_{1-x}Mg_xO_2$ (x = 0.00, 0.01, 0.02, 0.03, 0.04) nanoparticles.

the obtained values of the refractive index (n) and the real dielectric constant has the same values of n^2. The loss factor (dielectric loss tangent) was also estimated using the following equation [48].

$$\tan\delta = \frac{\varepsilon_1}{\varepsilon_2} \tag{11}$$

The relationship that exists between optical dielectric loss and photon energy for undoped TiO_2 and Mg doped TiO_2 were shown in Fig. 6(c). It was observed that tan δ changes with increasing in the Mg concentration in Mg doped TiO_2. The changes observed in the optical dielectric loss may be due to the formation of more free charges induced by Mg at the interfacial which increases the polarizability of the Mg doped TiO_2 [48].

The nonlinear properties of Mg doped TiO_2 can also be investigated by using already estimated linear optical parameters. The nonlinear optical properties of material have a remarkable scientific contribution to optoelectronic technologies such as optical signal processing, data storage, optical switching and electron-optic modulators [50,51]. For this reason, three significant nonlinear optical parameters, nonlinear refractive index n_2, first-order $\chi^{(1)}$ and third-order nonlinear susceptibilities $\chi^{(3)}$, for Mg doped TiO_2 can be estimated using following relations [50–52].

$$\chi^{(1)} = \frac{n_0^2 - 1}{4\pi},$$

$$\chi^{(3)} = B\left[\frac{n_0^2 - 1}{4\pi}\right]^4, \tag{12}$$

$$n_2 = \frac{12\pi\chi^{(3)}}{n_0}$$

where n_0 is the static refractive index can be found from the Wemple DiDomenico model analyses and B is a constant of 1.7×10^{-10} esu.

3.2.3. Photoluminescence studies

Photoluminescence (PL) techniques was employed to examine the electron–hole recombination features. PL emission is a valuable method to examine the migration and trapping efficacy of charge carriers, and to understand the recombination of electron–hole pairs [34]. P-L emission is achieved from the recombination of excited electrons and holes. PL of low intensity depicts a low recombination rate. Fig. 7 shows the PL spectra of $Mg_xT_{1-x}O_2$ (x = 0.00, 0.01, 0.02, 0.03, 0.04) doping concentration. It can be observed that the PL intensity of TiO_2 and is lower than that of undoped TiO_2. If TiO_2 is over doped, impurity band formed by the metal ions is expected to be the recombination center. Mg/TiO_2 with 4% doping concentration has the most intense PL intensity peak compared with the undoped and other doped samples at 397 nm. And it is well noted that as the doping concentration increases the peak intensity also increases. A wide P-L band was observed in the wavelength range of 424–462 nm which is as a result of Ov - oxygen vacancies and surface defects. The O-vacancies in the system lead to recombination. The UV peak emission at 397 nm matched together with the near band edge (NBE) emission of TiO_2, which is due to the recombination of free excitons through an exciton–exciton collision processes. These results show that the recombination of photo-generated electrons and holes is excellently curbed by Mg doping.

3.3. FESEM and EDX spectroscopy studies

The FESEM micrograph of undoped and Mg doped TiO_2 samples as revealed by Zeiss Ultra 55 were as shown in Fig. 8(a–c). It can be clearly observed from the micrograph that crystallite size of the samples decreases as Mg doping concentration increases, which falls in line with the estimated crystallite size in XRD analysis. The observation of

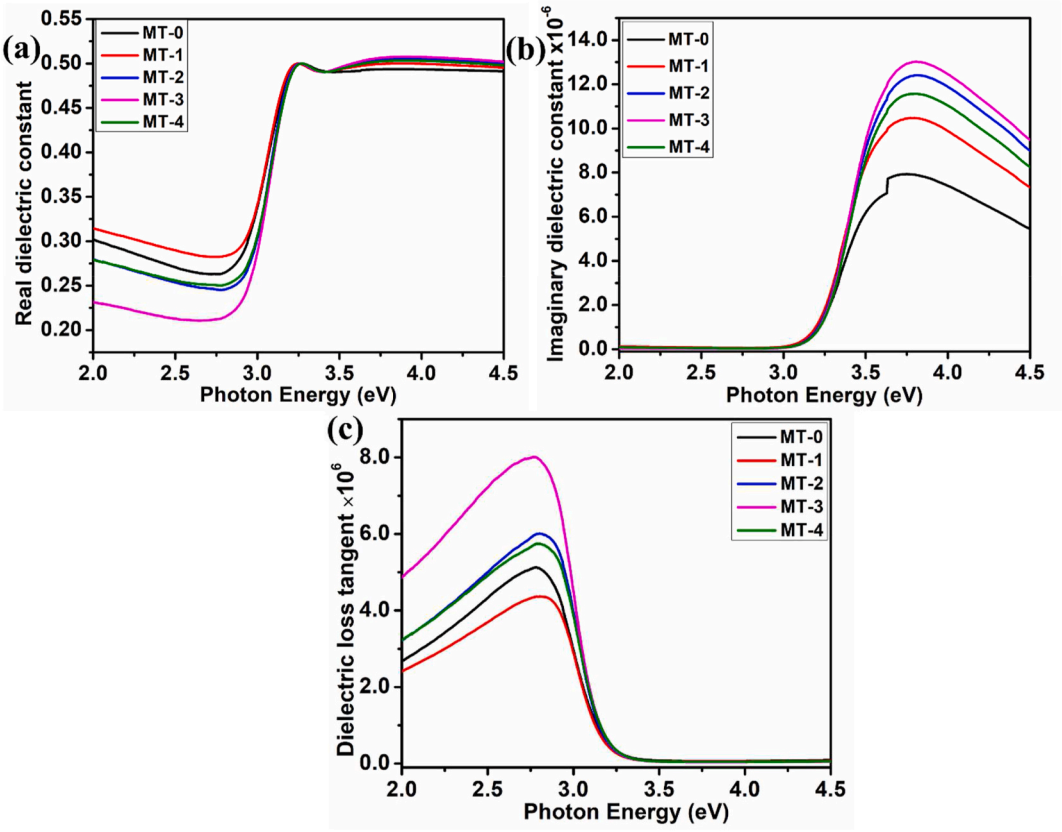


Fig. 6. (a) The real part of the dielectric constant (ε_1), (b) Imaginary part of the dielectric constant (ε_2) and (c) Optical dielectric loss tangent (tan δ) of undoped TiO_2 and Mg doped TiO_2.

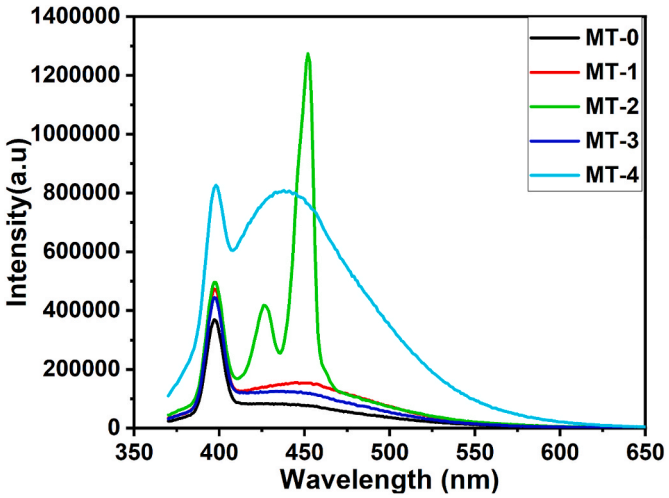


Fig. 7. Photoluminescence spectra of MT-0, MT-1, MT-2, MT-3 and MT-4.

decrease in crystallite size when the doping concentration was increased may be due to the fact that ionic radii of Mg^{2+} (0.71 Å) and Ti^{4+} (0.62 Å) are relatively close to each other, hence possible direct substitution of Mg^{2+} into the TiO_2 lattice [29]. The absence of impurity and broadening of the peak from the XRD peaks which occurred with increase in the dopant concentration, implies a reduction of crystallite size and increase in volume of unit cell. The micrograph also revealed the increment of grayish white patch dispersed on the surface of the samples with increase in Mg doping concentration which confirms that metal is incorporated in the TiO_2 lattice. The energy dispersive X-ray spectroscopy technique confirms that the pure TiO_2 contains oxygen (O) and Titanium (Ti) elements alone while Mg doped TiO_2 shows the presence of Carbon (C), Nitrogen (N), Oxygen (O), Magnesium (Mg), Molebdenum (Mo) and Titanium (Ti) as displayed in Fig. 8(d–f). The elements associated to host and dopants can be distinctly confirmed from these spectra also the atomic and weight percentages used to estimate the stoichiometry of the elements.

3.4. Magnetic properties of undoped and Mg doped TiO_2

The magnetic properties making use of VSM at room temperature were investigated for undoped and Mg doped TiO_2 nanoparticles. The plot of magnetization (M) against the magnetic field (H) of undoped and Mg-doped TiO_2 samples is displayed in Fig. 9. As shown in Fig. 9, all the samples analyzed show noticeable room temperature ferromagnetic (RTFM) characteristic as displayed from hysteresis loop with value of non-zero coercive field (Hc) and remanent magnetization (Mr). The observed results were on opposite of that reported by Ali et al. [34], for Mg doped TiO_2 nanoparticles samples prepared by sol-gel method at close range of Mg doping concentration. It was clearly shown that only their Mg doped TiO_2 exhibit soft ferromagnetic at room temperature. It is noteworthy to say that both pure and Mg TiO_2 anatase synthesized by sol gel method exhibit room temperature ferromagnetic (RTFTM) as shown in Fig. 9. From the plot of M versus H (Fig.

9), it can be noticed that saturation magnetization decreases with increase in magnetic moment on the incorporation of magnesium ions with exception of MT-2 sample which shows an increase in Ms-saturation magnetization. This substantial contribution of 2% Mg doped TiO_2 to the magnetic moment emanates from the surface defects like oxygen vacancy due to unpaired d electron of Ti^{3+}.

In addition, the observed RTFM characteristic for pure TiO_2 (MT-0) establishes the expected RTFM for undoped TiO_2 Nanoparticles. This behavior is exhibited due to high availability of defects and possibly

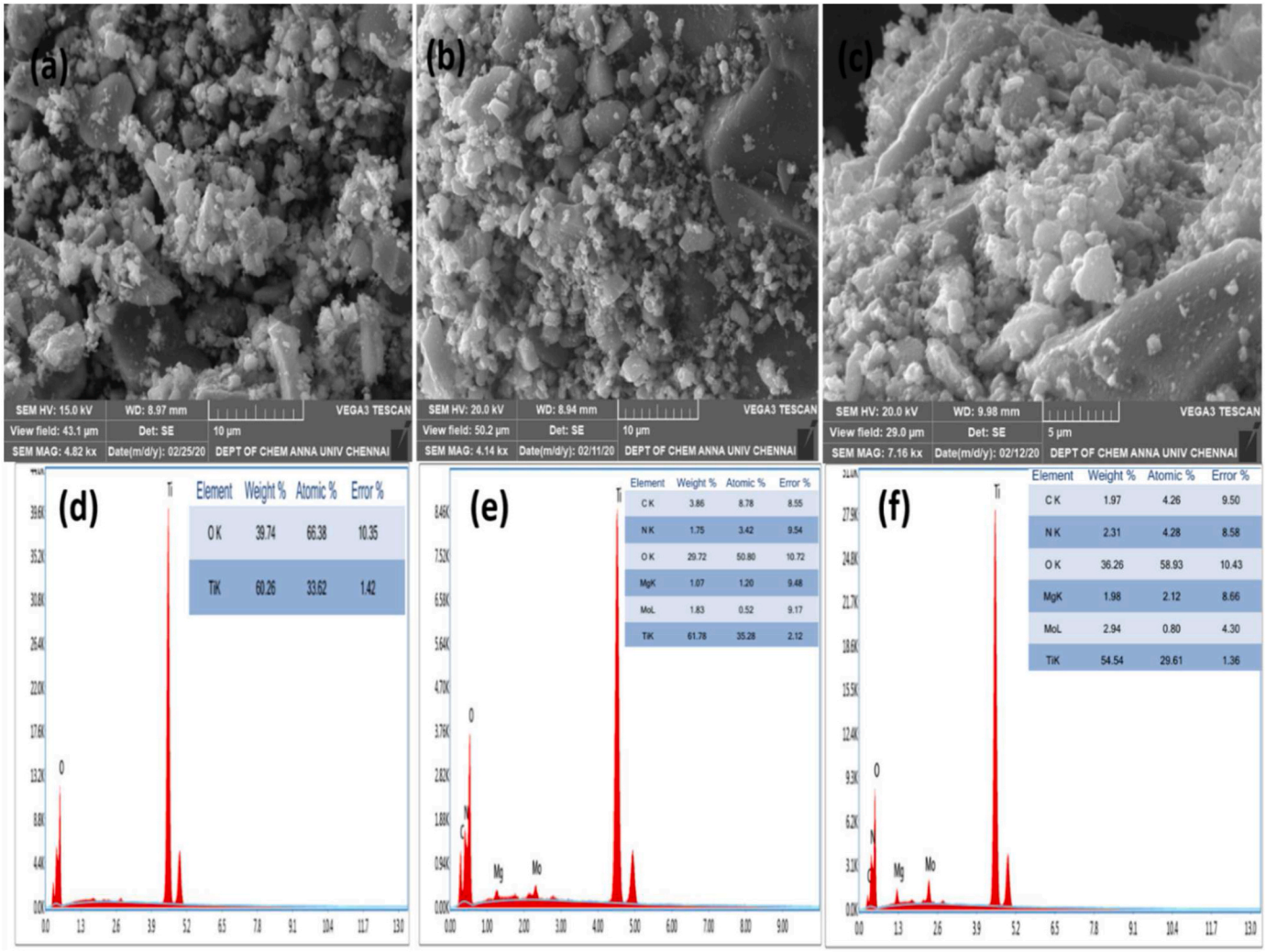


Fig. 8. (a–c) FESEM micrograph of MT-0, MT-2 and MT-4 (d–f) elemental composition of the as-prepared samples.

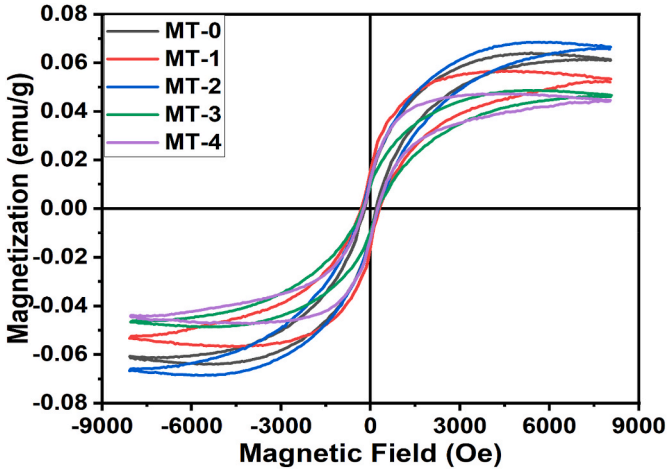


Fig. 9. Magnetization at room temperature against Magnetic field of pure and Mg-doped TiO_2 nanoparticles.

electrons could be trapping which leads to the promotion FM behavior in the undoped sample as reported by Mansour et al. [5].

The ferromagnetic observed in nanoparticles of pure and Mg doped TiO_2 could be ascribed to the Mg nanoclusters or defects formation and mobile charges (carriers) in the TiO_2 matrix. Hence, the identification of defect type accountable for RTFM still remains a major challenge to researchers. It has been reported that undoped TiO_2 FM behavior is remarkably related to vacancy oxygen than Ti vacancy defects [5,9,11]. The variations of characteristics of magnetic parameters with Mg concentration for the sample under investigation; saturation magnetization (M_s), remanent magnetization (M_r), coercive field (H_c) and the squareness (M_r/M_s), are anticipated as a result of the combination effects of alkaline earth-metal doping and oxygen vacancy defects.

Table 2 shows the ferromagnetic parameters dependency on pure and Mg doped TiO_2. FM has been generally proposed as a general characteristic common to inorganic nano-particles and trapped in the surface of nano-particles as published by Sundaresan and Rao [53]. The observed ferromagnetic in nano-particles of intrinsic and Mg doped TiO_2 can be ascribed to the Mg nanoclusters or the defects formation and

Table 2
Magnetic parameters of undoped and Mg-doped TiO_2 nanoparticles.

Samples	M_s (emu/g)×10^{-3}	M_r (emu/g)×10^{-3}	H_c (Oe)	$\frac{M_r}{M_s}$
MT-0	63.9	10.2	206.06	0.1596
MT-1	56.6	15.7	309.14	0.2774
MT-2	68.1	12.3	256.30	0.1806
MT-3	48.8	9.4	261.12	0.1926
MT-4	46.8	11.5	231.53	0.2457

mobile carrier charges in the TiO_2 matrix. Hence, the identification of defect type accountable for RTFM still remains a great challenge to researchers. It has been reported that undoped TiO_2 FM behavior is remarkably related to oxygen vacancy than Ti vacancy defects [5,9,11]. The variations of characteristics of magnetic parameters with Mg concentration for the sample under investigation; saturation magnetization (M_s), remanent magnetization (M_r), coercive field (H_c) and the squareness (M_r/M_s), are anticipated due to the combination effects of alkaline earth-metal doping and Ov defects.

We observed generally non-monotonic variations of M_s, M_r, H_c and M_r/M_s on Mg concentration in the samples. It has been reported that many factors governed the variation of magnetic moment by changing the concentration of dopant, for example, distribution of dopant ions randomly, increasing in dopant concentration by inhomogeneity of magnetization and formation of dopant clusters [5]. All these conditions have aggressive influence on the magnetic characteristics of the samples examined.

4. Conclusion

The study of structural, optical and magnetic studies of sol-gel synthesized Mg doped pure anatase TiO_2 nanoparticles have been investigated in this research. The structural formation of pure anatase phase of undoped and Mg doped Titanium dioxide were confirmed from XRD, Raman and FTIR analyses for all the investigated samples. Ultraviolet–Visible spectra(absorption) describe small blue change in the edge (absorption) of the samples doped, illustrating slight increase of optical band-gap, which can be employed for UV photocatalytic procedure. The photoluminescence-spectra of pure and doped samples revealed transitions electrons from conduction - valence band and the information of defect centers generated from Mg doping. These results showed that recombination of photogenerated holes and electrons was excellently curbed by Mg doping. The detailed morphological analysis using FESEM revealed the formation of the nanoparticles for undoped and Mg-doped TiO_2 samples. All synthesized nano-particle samples investigated gave a room temperature ferromagnetic (RTFM) characteristic revealed through evaluation of magnetization. The ferromagnetic parameters showed nonmonotonic variations with change of Mg concentration for the samples investigated. Such variations in their magnetic properties and Mg contents are due to competitively among factors governing the variation in magnetic moment with changing the dopant concentration. The cause of room temperature ferromagnetic behavior in the samples studied was majorly caused by defects like oxygen-vacancy due to incorporation of Mg into lattice of Titanium dioxide. Hence, RTFM induced make the synthesized samples an important material for future spintronic and optoelectronic technologies.

Credit authors statement

O. Adedokun: Investigation, Conceptualization, Data curation, Writing– original draft. P. Sivaprakash: Investigation, Data curation, Formal analysis, Writing – review & editing, A.S. Ajani: Formal analysis, Writing – review & editing, I.T. Bello: Formal analysis, Writing – review & editing, S. Arumugam: Supervision, Conceptualization, Project administration, Writing – review & editing.

Declaration of competing interest

The authors declare that they have no known competing financial interests or personal relationships that could have appeared to influence the work reported in this paper.

Data availability

Data will be made available on request.

Acknowledgement

O. Adedokun gratefully acknowledges the Department of Science & Technology (Govt. of India) for the award of 2019/2020 Research Training Fellowship for Developing Countries Scientist (RTF-DCS). The authors acknowledge with gratefulness the Centre for High-Pressure Research, Bharathidasan University, India for sample characterizations.

References

[1] A. Stylianou, S. Kontomaris, C. Grant, E. Alexandratou, Review article atomic force microscopy on biological materials related to pathological conditions, Scanning (2019) 1–25, 2019.
[2] A. Janotti, C.G. Van De Walle, Fundamentals of zinc oxide as a semiconductor, Rep. Prog. Phys. 72 (2009) 1–29, https://doi.org/10.1088/0034-4885/72/12/126501.
[3] B. O'regan, M. Grfitzeli, A low-cost, high-efficiency solar cell based on dye-sensitized, Nature 353 (1991) 737–740.
[4] B. Santara, B. Pal, P.K. Giri, Signature of strong ferromagnetism and optical properties of Co doped TiO 2 nanoparticles, J. Appl. Phys. 110 (2011), https://doi.org/10.1063/1.3665883.
[5] S.A. Mansour, A.H. Farha, M.F. Kotkata, Sol–gel synthesized Co-doped anatase TiO2 nanoparticles: structural, optical, and magnetic characterization, J. Inorg. Organomet. Polym. Mater. 29 (2019) 1375–1382, https://doi.org/10.1007/s10904-019-01102-6.
[6] J. Wei, J.X. Liu, Y.C. Dang, K. Xu, Y. Zhou, A review of nanostructured TiO2 application in Li-Ion batteries, in: Adv. Mater. Res., 2013, pp. 301–306. https://dx.doi.org/10.4028/www.scientific.net/AMR.750-752.301.
[7] G.A. Alamu, O. Adedokun, I.T. Bello, Y.K. Sanusi, Plasmonic enhancement of visible light absorption in Ag-TiO2 based dye-sensitized solar cells, Chem. Phys. Impact 3 (2021), 100037, https://doi.org/10.1016/j.chphi.2021.100037.
[8] J. Schneider, M. Matsuoka, M. Takeuchi, J. Zhang, Y. Horiuchi, M. Anpo, D. W. Bahnemann, Understanding TiO2photocatalysis: mechanisms and materials, Chem. Rev. 114 (2014) 9919–9986, https://doi.org/10.1021/cr5001892.
[9] C. Gómez-Polo, S. Larumbe, J.M. Pastor, Room temperature ferromagnetism in non-magnetic doped TiO2 nanoparticles, in: J. Appl. Phys., 2013, https://doi.org/10.1063/1.4795615.
[10] Y. Matsumoto, M. Murakami, T. Shono, T. Hasegawa, T. Fukumura, M. Kawasaki, P. Ahmet, T. Chikyow, S.Y. Koshihara, H. Koinuma, Room-temperature ferromagnetism in transparent transition metal-doped titanium dioxide, Science 291 (2001) 854–856, https://doi.org/10.1126/science.1056186 (1979).
[11] V.R. Akshay, B. Arun, G. Mandal, M. Vasundhara, Structural, optical and magnetic behavior of sol-gel derived Ni-doped dilute magnetic semiconductor TiO2 nanocrystals for advanced functional applications, Phys. Chem. Chem. Phys. 21 (2019) 2519–2532, https://doi.org/10.1039/c8cp06875e.
[12] B. Ghosh, M. Sardar, S. Banerjee, Destruction of ferromagnetism in Cu-doped ZnO upon annealing: role of oxygen vacancy, in: AIP Conf. Proc., 2012, pp. 1231–1232, https://doi.org/10.1063/1.4710456.
[13] K. Dodge, J. Chess, J. Eixenberger, G. Alanko, C.B. Hanna, A. Punnoose, Role of oxygen defects on the magnetic properties of ultra-small Sn 1-xFexO2 nanoparticles, in: J. Appl. Phys., 2013, https://doi.org/10.1063/1.4794140.
[14] S.A. Ahmed, Annealing effects on structure and magnetic properties of Mn-doped TiO2, J. Magn. Magn Mater. 402 (2016) 178–183, https://doi.org/10.1016/j.jmmm.2015.11.065.
[15] M.A. Kareem, I.T. Bello, H.A. Shittu, P. Sivaprakash, O. Adedokun, S. Arumugam, Synthesis, characterization, and photocatalytic application of silver doped zinc oxide nanoparticles, Clean. Mater. 3 (2022), 100041, https://doi.org/10.1016/j.clema.2022.100041.
[16] H.A. Shittu, O. Adedokun, M.A. Kareem, P. Sivaprakash, I.T. Bello, S. Arumugam, Effect of low-doping concentration on silver-doped SnO2 and its photocatalytic applications, Biointerface Res. Appl. Chem. 13 (2023) 1–15, https://doi.org/10.33263/BRIAC132.165.
[17] R. Parra, M.S. Góes, M.S. Castro, E. Longos, P.R. Bueno, J.A. Varela, Reaction pathway to the synthesis of anatase via the chemical modification of titanium isopropoxide with acetic acid, Chem. Mater. 20 (2008) 143–150, https://doi.org/10.1021/cm702286e.
[18] R. Gunnarsson, U. Helmersson, I. Pilch, Synthesis of titanium-oxide nanoparticles with size and stoichiometry control, J. Nanoparticle Res. 17 (2015), https://doi.org/10.1007/s11051-015-3158-3.
[19] G. Ali, H.J. Kim, J.M. Kum, S.O. Cho, Rapid synthesis of TiO2 nanoparticles by electrochemical anodization of a Ti wire, Nanotechnology 24 (2013), https://doi.org/10.1088/0957-4484/24/18/185601.
[20] H. Rasoulnezhad, G. Hosseinzadeh, R. Hosseinzadeh, N. Ghasemian, Preparation of transparent nanostructured N-doped TiO2 thin films by combination of sonochemical and CVD methods with visible light photocatalytic activity, J. Adv. Ceram. 7 (2018) 185–196, https://doi.org/10.1007/s40145-018-0270-8.
[21] W.J. Aziz, S.Q. Ali, N.Z. Jassim, Production TiO2 nanoparticles using laser ablation in ethanol, Silicon 10 (2018) 2101–2107, https://doi.org/10.1007/s12633-017-9730-y.
[22] H.F. Mehnane, C. Wang, K.K. Kondamareddy, W. Yu, W. Sun, H. Liu, S. Bai, W. Liu, S. Guo, X.Z. Zhao, Hydrothermal synthesis of TiO2 nanoparticles doped with trace amounts of strontium, and their application as working electrodes for dye sensitized solar cells: tunable electrical properties & enhanced photo-conversion

performance, RSC Adv. 7 (2017) 2358–2364, https://doi.org/10.1039/c6ra26012h.
[23] A.E. Danks, S.R. Hall, Z. Schnepp, The evolution of "sol-gel" chemistry as a technique for materials synthesis, Mater. Horiz. 3 (2016) 91–112, https://doi.org/10.1039/c5mh00260e.
[24] R. Zahid, M. Manzoor, A. Rafiq, M. Ikram, M. Nafees, A.R. Butt, S.G. Hussain, S. Ali, Influence of iron doping on structural, optical and magnetic properties of TiO2 nanoparticles, Electron. Mater. Lett. 14 (2018) 587–593, https://doi.org/10.1007/s13391-018-0060-z.
[25] Y. Wang, J. Ma, J.P. Zhou, X.M. Chen, J.Z. Wang, First-principles study of the electronic structure of nonmetal-doped anatase TiO2, J. Kor. Phys. Soc. 68 (2016) 409–414, https://doi.org/10.3938/jkps.68.409.
[26] X. Zhu, L. Pei, R. Zhu, Y. Jiao, R. Tang, W. Feng, Preparation and characterization of Sn/La co-doped TiO2 nanomaterials and their phase transformation and photocatalytic activity, Sci. Rep. 8 (2018), https://doi.org/10.1038/s41598-018-30050-3.
[27] N. Rajamanickam, S.S. Kanamni, S. Rajashabala, K. Ramachandran, Influence of Sr doping on structural, optical and magnetic properties of TiO2 nanoparticles, Mater. Lett. 161 (2015) 520–522, https://doi.org/10.1016/j.matlet.2015.09.023.
[28] N. Nithyaa, N.V. Jaya, Structural, optical, and magnetic properties of Gd-doped TiO2 nanoparticles, J. Supercond. Nov. Magnetism 31 (2018) 4117–4126, https://doi.org/10.1007/s10948-018-4693-9.
[29] J.O. Olowoyo, M. Kumar, N. Singhal, S.L. Jain, J.O. Babalola, A.V. Vorontsov, U. Kumar, Engineering and modeling the effect of Mg doping in TiO2 for enhanced photocatalytic reduction of CO2 to fuels, Catal. Sci. Technol. 8 (2018) 3686–3694, https://doi.org/10.1039/c8cy00987b.
[30] D. Chen, D. Yang, Q. Wang, Z. Jiang, Effects of boron doping on photocatalytic activity and microstructure of titanium dioxide nanoparticles, Ind. Eng. Chem. Res. 45 (2006) 4110–4116, https://doi.org/10.1021/ie0600902.
[31] J.L. Luo, S.F. Wang, W. Liu, C.X. Tian, J.W. Wu, X.T. Zu, W.L. Zhou, X.D. Yuan, X. Xiang, Influence of different aluminum salts on the photocatalytic properties of Al doped TiO2 nanoparticles towards the degradation of AO7 dye, Sci. Rep. 7 (2017), https://doi.org/10.1038/s41598-017-08216-2.
[32] Q. Hou, W. Li, C. Li, X. Jia, C. Zhao, Effects of carbon doping and vacancy defect on the magnetism of anatase TiO2, Phys. Lett., Section A: Gen., Atom. and Solid State Physics 383 (2019) 186–195, https://doi.org/10.1016/j.physleta.2018.10.028.
[33] Y. Liu, W. Zhou, P. Wu, Room-temperature ferromagnetism and optical properties in Mg-doped TiO 2: a density functional theory investigation, J. Appl. Phys. 115 (2014), https://doi.org/10.1063/1.4870237.
[34] T. Ali, A. Ahmed, M.N. Siddique, U. Alam, M. Muneer, P. Tripathi, Influence of Mg2 + ion on the optical and magnetic properties of TiO2 nanostructures: a key role of oxygen vacancy, Optik (Stuttg) 223 (2020), https://doi.org/10.1016/j.ijleo.2020.165340.
[35] L. Chouhan, S.K. Srivastava, Observation of room temperature d0 ferromagnetism, band-gap widening, zero dielectric loss and conductivity enhancement in Mg doped TiO2 (rutile + anatase) compounds for spintronics applications, J. Solid State Chem. 307 (2022), https://doi.org/10.1016/j.jssc.2021.122828.
[36] S. Sen, An X-ray line broadening analysis in the vacuum evaporated silver films, Jpn., Phys. Soc. Jpn. (1975) 1641–1647.
[37] A. Weibel, R. Bouchet, F. Boulc'h, P. Knauth, The big problem of small particles: a comparison of methods for determination of particle size in nanocrystalline anatase powders, Chem. Mater. 17 (2005) 2378–2385, https://doi.org/10.1021/cm0403762.
[38] P.M. Kibasomba, S. Dhlamini, M. Maaza, C.P. Liu, M.M. Rashad, D.A. Rayan, B. W. Mwakikunga, Strain and grain size of TiO2 nanoparticles from TEM, Raman spectroscopy and XRD: the revisiting of the Williamson-Hall plot method, Results Phys. 9 (2018) 628–635, https://doi.org/10.1016/j.rinp.2018.03.008.
[39] P. Scherrer, Bestimmung der Grosse und der Inneren Struktur von Kolloidteilchen Mittels Rontgenstrahlen, Nachrichten von der Gesellschaft der Wissenschaften, Gottingen, Math.-Phys. Kl. 2 (1918) 98–100.
[40] Y. Z, Q.C.W.F. Zhang, Y.L. He, M.S. Zhang, Raman scattering study on anatase TiO2 nanocrystals, J. Phys. D Appl. Phys. 33 (2000) 912.
[41] W. Ma, Z. Lu, M. Zhang, Investigation of structural transformations in nanophase titanium dioxide by Raman spectroscopy, Appl. Phys. Mater. Sci. Process 66 (1998) 621–627, https://doi.org/10.1007/s003390050723.
[42] A. Kumar, M.K. Kashyap, N. Sabharwal, S. Kumar, A. Kumar, P. Kumar, K. Asokan, Structural, optical and weak magnetic properties of Co and Mn codoped TiO2 nanoparticles, Solid State Sci. 73 (2017) 19–26, https://doi.org/10.1016/j.solidstatesciences.2017.09.002.
[43] H.P. Shivaraju, G. Midhun, K.M. Anil Kumar, S. Pallavi, N. Pallavi, S. Behzad, Degradation of selected industrial dyes using Mg-doped TiO2 polyscales under natural sun light as an alternative driving energy, Appl. Water Sci. 7 (2017) 3937–3948, https://doi.org/10.1007/s13201-017-0546-0.
[44] T. Siva Rao, T.A. Segne, T. Susmitha, A. Balaram Kiran, C. Subrahmanyam, Photocatalytic degradation of dichlorvos in visible light by mg 2+-tio2 nanocatalyst, Adv. Mater. Sci. Eng. 2012 (2012), https://doi.org/10.1155/2012/168780.
[45] J. Tauc, Optical properties of amorphous semiconductors, in: Amorphous and Liquid Semiconductor, 1974, pp. 159–220.
[46] J. Manju, S.M.J. Jawhar, Synthesis of magnesium-doped TiO2 photoelectrodes for dye-sensitized solar cell applications by solvothermal microwave irradiation method, J. Mater. Res. 33 (2018) 1534–1542, https://doi.org/10.1557/jmr.2018.115.
[47] A. Khorsand Zak, A. Manaf Hashim, M. Darroudi, Optical Properties of ZnO/BaCO 3 Nanocomposites in UV and Visible Regions, 2014. http://www.nanoscalereslett.com/content/9/1/399.
[48] T.A. Hameed, A.A. Azab, R.S. Ibrahim, K.E. Rady, Optimization, structural, optical and magnetic properties of TiO2/CoFe2O4 nanocomposites, Ceram. Int. 48 (2022) 20418–20425, https://doi.org/10.1016/j.ceramint.2022.03.327.
[49] M. Isik, N.M. Gasanly, Linear and nonlinear optical properties of Bi12GeO20 single crystal for optoelectronic applications, Mater. Sci. Semicond. Process. 153 (2023), https://doi.org/10.1016/j.mssp.2022.107170.
[50] Y. Wang, D. Sun, J. Chen, C. Shen, G. Liu, D. Wang, S. Wang, Linear and nonlinear optical characteristics effected by Na+ ions of low concentration for potassium dihydrogen phosphate crystal, Optik (Stuttg). 251 (2022), https://doi.org/10.1016/j.ijleo.2021.168481.
[51] Z.R. Khan, K.V. Chandekar, A. Khan, N. Akhter, M.A. Sayed, M. Shkir, H. Algarni, S. AlFaify, An impact of novel Terbium (Tb) doping on key opto-nonlinear optical characteristics of spray pyrolyzed NiO nanostructured films for opto-nonlinear applications, Mater. Sci. Semicond. Process. 138 (2022), https://doi.org/10.1016/j.mssp.2021.106260.
[52] V. Ganesh, I.S. Yahia, S. AlFaify, M. Shkir, Sn-doped ZnO nanocrystalline thin films with enhanced linear and nonlinear optical properties for optoelectronic applications, J. Phys. Chem. Solid. 100 (2017) 115–125, https://doi.org/10.1016/j.jpcs.2016.09.022.
[53] A. Sundaresan, C.N.R. Rao, Ferromagnetism as a universal feature of inorganic nanoparticles, Nano Today 4 (2009) 96–106, https://doi.org/10.1016/j.nantod.2008.10.002.